Molecular Crystals and Liquid Crystals

ISSN: 1542-1406 (Print) 1563-5287 (Online) Journal homepage: http://www.tandfonline.com/loi/gmcl20

# 8.1 Å Resolution Cryo-EM Structure of Lumbricus terrestris Hemoglobin Provides Insight into the Complex Assembly

Wei-Ting Chen, Yu-Chuen Chen, Szu-Hua Chen & Chih-Yu Chao

**To cite this article:** Wei-Ting Chen, Yu-Chuen Chen, Szu-Hua Chen & Chih-Yu Chao (2015) 8.1 Å Resolution Cryo-EM Structure of Lumbricus terrestris Hemoglobin Provides Insight into the Complex Assembly, Molecular Crystals and Liquid Crystals, 612:1, 220-231, DOI: 10.1080/15421406.2015.1031583

**To link to this article:** http://dx.doi.org/10.1080/15421406.2015.1031583

Published online: 06 Jul 2015.

*Mol. Cryst. Liq. Cryst.*, Vol. 612: pp. 220–231, 2015

ISSN: 1542-1406 print/1563-5287 online
DOI: 10.1080/15421406.2015.1031583



# 8.1 Å Resolution Cryo-EM Structure of Lumbricus terrestris Hemoglobin Provides Insight into the Complex Assembly

WEI-TING CHEN,[1,3] YU-CHUEN CHEN,[3] SZU-HUA CHEN,[3] AND CHIH-YU CHAO[1,2,3,*]

[1]Department of Physics, National Taiwan University, Taipei, Taiwan
[2]Graduate Institute of Applied Physics, National Taiwan University, Taipei, Taiwan
[3]Biomedical & Molecular Imaging Center, National Taiwan University College of Medicine, Taipei, Taiwan

*The iron-containing hemoglobins (Hbs) are essential proteins to serve as oxygen transporters in the blood. The cooperative oxygen-binding is a distinct feature for them to load and unload oxygen efficiently. Among various kinds of hemoglobins, the earthworm hemoglobins are the champions in carrying oxygen due to not only their large size but also the unusually high cooperativity. Here we report the first study on the cooperative mechanism in the Lumbricus terrestris hemoglobin. The near atomic resolution of our cryo-EM structure also enables us to further visualize the additional sinusoidal bracelet, which accounts for a new assembly mechanism of this enormous structure.*

**Keywords** Hemoglobin; Earthworm; Cryo-EM; Allosteric cooperativity; Assisted assembly

## 1. Introduction

We all need oxygen ($O_2$), and so do most animals. The most widely distributed oxygen-carrying proteins in the animal kingdom are the iron-containing hemoglobins (Hbs). The remarkable cooperative binding ability of Hb and the allosteric communication between each binding site have fascinated scientists for more than a century. For tetrameric human Hb, the small shift of iron (Fe) position in the heme group, due to ligation of oxygen, results in large quaternary transitions [1]. In contrast, no structural changes induced by ligand-binding have been determined in the giant hexagonal-bilayer earthworm Hb until now. The design of such huge macromolecular assembly has attracted scientists' attentions for nearly two centuries.

The earthworm *L. terrestris* Hb was the first protein to be crystallized in 1840 [2]. It consists of 144 separate oxygen-binding globin subunits and 36 non-heme linker chains, where the linker chains stitch all the globin subunits together into one large assembly.

*Address correspondence to Chih-Yu Chao, Department of Physics, National Taiwan University, Taipei 10617, Taiwan. E-mail: cychao@ntu.edu.tw

Color versions of one or more of the figures in the article can be found online at www.tandfonline.com/gmcl.

Many structural studies by electron microscopy [3–5] and X-ray crystallography [6–8] have paved the way for a deeper understanding of this interesting molecular machine. The 3.5 Å resolution crystal structure of *L. terrestris* Hb reported by Royer and co-workers [6] is a remarkable milestone. This structure provides the first atomic model for an entire megadalton respiratory protein, and reveals detailed hierarchical arrangement of 180 polypeptide chains. However, very little is known about the cooperative mechanism of oxygen binding and about the structural transitions induced by different ligand binding.

The most intriguing functional characteristic of *L. terrestris* Hb is the unusually high cooperativity of oxygen binding (Hill coefficient = 7.9, under conditions of maximum cooperativity) [9], but no detectable structural change upon oxygenation was observed by resonance Raman spectra [10] and small angle X-ray scattering [11]. The other interesting and recurring issue concerns the presence of a central subunit in the *L. terrestris* Hb. Ohtsuki and Crewe [12] provided the first evidence for the central substructure in the *L. terrestris* Hb. The "bracelet model" proposed by Vinogradov *et al.* [13] described the role of the central bracelet to act as linkers between globin subunits. Then the 5.5 Å resolution crystal structure [8] revealed that the central subunits are formed by the N-terminal triple-stranded coiled coils of the linker chains. However, the smaller central cavity observed in some cryo-EM structures [5,14,15] and the sinusoidal pillars observed in the 14.9 Å cryo-EM structure [3] imply the existence of additional central densities which are still absent in the X-ray structure.

In this paper, we report the 8.1 Å resolution cryo-EM structure of the entire *L. terrestris* Hb in the oxygenated form, which provides the first near-atomic resolution structure for this protein in its native state. By using flexible fitting of previously reported crystal structure to our cryo-EM reconstruction, we construct a pseudo-atomic model for high-resolution description of the subunit arrangement in the oxygenated state. Comparison of the conformation of the *L. terrestris* Hb between two different functional states reveals tertiary and quaternary allostery in the heme pocket and an alteration of the overall size of this complex which provide clues to the cooperative mechanism. Moreover, the electron densities of additional sinusoidal bracelet are clearly visible in our cryo-EM data, and this discovery may account for a new assembly mechanism of the whole Hb complex.

## 2. Experimental Details

The Hbs were purified from the blood of the common earthworm *Lumbricus terrestris*. Live earthworms were washed in distilled water to remove dirt and mucus, dried off, and cut near the seventh body segment. The blood was collected via capillary tubes into a centrifugal tube containing 0.1 M Tris-HCl buffer, pH 7.0, 1 mM EDTA. The collected blood was centrifuged at 20,000 $\times$ *g* for 0.5 hr at 4 degrees Celsius to remove any cell debris and particulate matter. The supernatant was then centrifuged at 150,000 $\times$ *g* for 2 hr at 4 degrees Celsius. The red pellet was dissolved in 0.1 M Tris-HC1 buffer, pH 7.0, 1 mM EDTA, 2 mM phenylmethanesulfonyl fluoride (PMSF) [16].

For cryo-EM, the Hb sample was dialyzed against a 50 mM Tris-HCl buffer, pH 7.2, 10 mM $CaCl_2$, 10 mM $MgCl_2$ to a concentration of 2 mg/ml. Approximately 3.5 $\mu$l of the sample dilution was applied onto holey carbon side of each freshly glow-discharged Quantifoil copper grid (Quantifoil Micro Tools GmbH, Jena, Germany). After blotting at room temperature for 4 s at 100% humidity in the Vitrobot (FEI, Netherlands), the grid was rapidly plunged into liquid ethane cooled by liquid nitrogen.

Grids of frozen hydrated samples were transferred into the electron microscope by using the Gatan 626 cryo-transfer system (Gatan, USA). The cryo specimens were imaged in a TF20 (FEI, Netherlands) electron microscope operated at an acceleration voltage of 200 kV. Images were recorded at a nominal magnification of 80,000 using a Gatan 4k × 4k CCD camera (Gatan, USA) by an automated data acquisition system, Leginon [17].

The quality of the CCD images were determined by their power spectra. Micrographs with noticeable drift, charging or astigmatism were discarded. The defocus and astigmatism parameters of each micrograph were determined using the program CTFFIND3 [18], and the contrast transfer function (CTF) correction was done with the module CTF2D-FLIP from IMAGIC [19]. All the particles without contaminants and aggregates were semi-automatically selected using the EMAN2 tool e2boxer [20]. Approximately 6,000 particles were selected from 250 micrographs. The initial map was calculated from class averages by angular reconstitution with D6 symmetry imposed and then refined by twelve cycles of projection matching procedure implemented in IMAGIC with a progressively decreased angular increment (with a final value of $1^\circ$ only).

The 3D volume was analyzed, segmented and visualized by UCSF Chimera [21]. The CO-binding crystal structure (PDB code: 2GTL) protomer was first rigid-body fitted into the segmented cryo-EM map by Chimera. Then the conformation refinement was performed by the simulated annealing molecular dynamics optimization protocol embedded in the Flex-EM software [22]. During the flexible fitting process, the secondary structural elements detected by RIBFIND [23] were assigned as rigid bodies. The simulated annealing molecular dynamics were performed by gradually increasing the temperature from 0K to 1000K and decreasing it back to 0K. The coordinates of the rigid bodies were displaced in the direction which maximized their cross-correlations with the cryo-EM density map. The optimization is terminated if the change in cross correlation function is $< 0.001$. After the protomer structure was flexibly fitted into the cryo-EM density map, the whole map was symmetrically fitted by UCSF Chimera.

## 3. Results

### *8.1 Å Resolution Cryo-EM Map of* L. terrestris *Hb*

We carried out single particle cryo-EM analysis of *L. terrestris* Hb in its oxygenated state (Figure 1(a) and 1(b)). No reference was made during the reconstruction process to avoid introducing model bias. The final 3D reconstruction is presented in Figure 1, with one colored protomer. The map resolution was 8.1 Å according to the $FSC_{1/2\text{-bit}}$ criterion (Figure 1(e)). At 8 Å resolution, all the 144 globin subunits and 36 linker chains can be unambiguously assigned. The 36 non-heme linker chains formed a central core which acted as a scaffold covered by 144 oxygen binding globins. Two unique dyad axes designated "Q" and "P" (Figure 1(b), 1(c) and 1(d)) oriented every $30^\circ$ in the central plane reflected the D6 symmetry of the complex. The higher resolution of our cryo-EM map allows a clear visualization of each $\alpha$-helix in the N-terminal triple-stranded coiled coils. This allowed unambiguous assignment of three linker chains, designated L1, L2, and L3 based on the known crystal structure.

### *Structural Fitting*

We extracted the protomer from the complex (Figure 2(a) and 2(b)) and rigid-body docked the CO-binding form of *L. terrestris* Hb crystal structure into it. As the rigid body docking

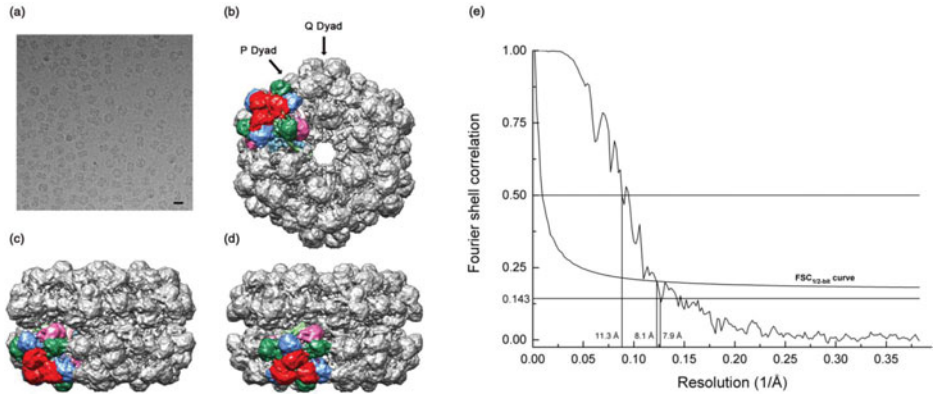


**Figure 1.** Final reconstruction of *Lumbricus terrestris* Hb at 8.1 Å resolution with one colored protomer. (a) A cryo-EM image of *Lumbricus terrestris* Hbs. Scale bar corresponds to 30 nm. (b) Top view along the molecular 6-fold axis. Individual subunits are shown in different colors, with a subunits in cornflower blue, b subunits in hot pink, c subunits in sea green, d subunits in red, linker chain L1 in light green, L2 in sky blue, and L3 in pink. Arrows point to the Q- and P-dyad axes. (c) The whole molecule viewed along a Q-dyad axis. (d) The whole molecule viewed along a P-dyad axis. (e) Resolution determination by Fourier shell correlation of two maps calculated separately from two halves of the dataset. The estimated resolution of *L. terrestris* Hb was 8.1 Å according to the $FSC_{1/2\text{-bit}}$ criterion.

is performed using the entire protomer, the colied coil domain matches well, however, significant discrepancies are observed in the globin subunits and the $\beta$ barrel domains. The overall cross-correlation coefficients is 0.70. The discrepancies between the $O_2$-binding cryo-EM map and the CO-binding crystal structure suggested a conformational change induced by different ligand binding. To analyze the domain movements more accurately, we used flexible fitting protocol Flex-EM [22] to dock the crystal structure into our EM map. This method maintains the connectivity between the domains and optimizes the position and orientation of each defined rigid body segment simultaneously [23]. The model for the protomer fits tightly into the density map (see Figure 2(c)and 2(d)), except for some loop regions. The most remarkable discrepancies involve the extra densities in the N-terminal coiled coil domain. Compared to the crystal structure, the L1 linker chain is N-terminally extended by a unique tail domain (Figure 2(d)), and finally forms a bracelet structure around the center of the assembled complex.

After the protomer structure was flexibly docked into the density map, the whole map was symmetrically fitted by taking into account clashes between symmetrically placed molecules. The very high similarity between the density map and the flexible-fitting structure (cross-correlation coefficients $\sim$ 0.94) allowed us to construct a pseudo-atomic model of the observed hexamer in the oxygen-binding state. With this approach, we were able to model the conformational change induced by oxygen binding. The obtained oxygen-bound structure of *L. terrestris* Hb provides a different state to enable us to investigate in detail the effect of different ligand binding. Figure 3 shows the comparison of the *L. terrestris* Hb models in the $O_2$-bound and CO-bound states. Upon binding of the oxygen molecules, each of the protomers moves outward along the quasi 3-fold axis, causing a radial expansion of the hexagonal bilayer complex. The fitted pseudo-atomic model has a diameter of 303 Å and a height of 194 Å. On the inside, the cavity of the hexamer after oxygen binding is

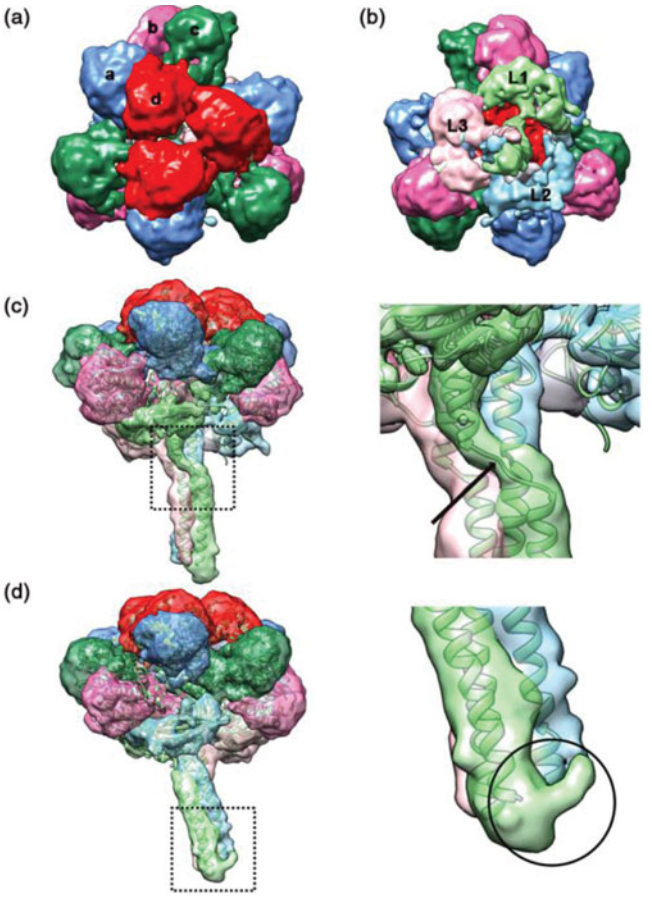


**Figure 2.** Cryo-EM density map and flexible fit of one protomer. (a) Top view along the pseudo three-fold axis shown colored as in Figure 1. (b) Bottom view along the pseudo three-fold axis. The triple-stranded stalk can be seen from this view. (c) Side view of one protomer along the L1 linker chain. Arrow indicates the inter-helical loop of L1. (d) Side view along the L2 linker chain. Extra density is visible at the N terminus of L1 linker chain (black circle).

47 Å in diameter and remains almost unchanged. Even though the inside cavity diameter of the CO-bound crystal structure still matches that of the $O_2$-bound complex, the outside diameter is 15 Å narrower in CO-binding state. The error margin of the pseudo-atomic model depends on the accuracy of docking. For a map at 10 Å resolution, the $\alpha$-carbon root-mean-square deviation is about 2–4 Å [22]. For our 8.1 Å resolution map, the error margin will be about 2.5 Å.

Each of 12 protomers is composed of a globin dodecamer which binds to the head of a linker heterotrimer. The twelve globin subunits $(abcd)_3$ in each protomer appear to group into six peanut-like subunit pairs (a-d, b-c) that create a pseudo three-fold symmetry (Figure 2(a)), whereby each protomer is considered to be a trimer of tetramers. The L1, L2, and L3 linker chains are held together as a trimer by disulfide bonds and strong hydrophobic interactions [6]. Each linker chain is comprised of a long N-terminal $\alpha$ helix, a low-density lipoprotein receptor (LDLR)-like domain [24], and a typical eight-stranded $\beta$ barrel domain

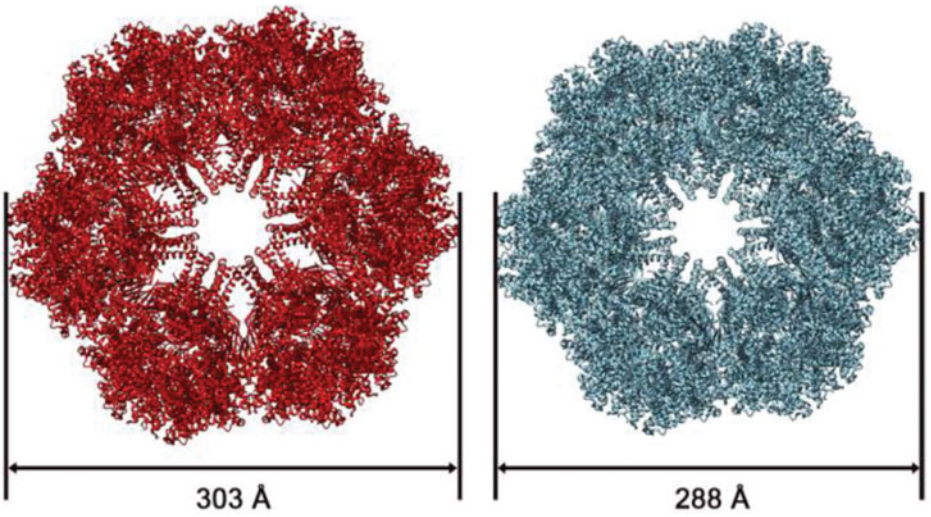


**Figure 3.** Comparison between the CO-bound state (cyan) and $O_2$-bound state (red) of the *Lumbricus terrestris* Hb models.

[6]. A nonhelical region divides the N-terminal $\alpha$ helix into a long coiled coil and a shorter one near the $\beta$ barrel domain [25]. It was also known that linker chain L1 exhibits the longest inter-helical segment which introduces a break in the crystal structure [25]. Thus, we refined the inter-helical loop by generating additional possible conformations [26] which fit our density map more accurately (Figure 2(c)).

### *Central Linker Complex*

The linker trimer has a long stalk at the center of *L. terrestris* Hb, formed from the triple-stranded coiled coil. The coiled coil domains provide the primary contacts between one-twelfth protomers that form the overall hexagonal bilayer structure. At this resolution, the triple-stranded coiled coils were clearly evident. In order to demonstrate the arrangement of the 36 linker chains at the core of the complex, we masked out the globin subunits and a portion of the linker chains (Figure 4(a)). Then we found that the two hexagonal rings are staggered, so that the stalks appear curved between the top and bottom rings when viewed from the Q dyad (Figure 4(b)). Each triple-stranded stalk projected from outside toward the main plane of the central linker complex (Figure 4(c)) are arranged in an alternating manner. The angle between the top and bottom stalks is approximately 45° (Figure 4(b)). Interestingly, our map also reveals additional densities in the N termini of the linker chains, which make the central cavity much smaller than that of the X-ray structure. The extra density forms a bracelet structure which connects all the coiled coil domains of L1 and L2 linker chains in the assembled complex (Figure 4(a)). These features are totally absent in the X-ray structure for unknown reasons [3].

The interdigitation between the extra density and the L1, L2 coiled coils can be appreciated from the unwrapped planar map (Figure 4(a)). As shown in the unrolled central linker complex, the extra density appears as a continuous sinusoid which was presented as six sinusoidal pillars in the 14.9 Å cryo-EM structure [3]. To further investigate the changes occurred in the coiled coil domain, we compare the extracted coiled coil structures

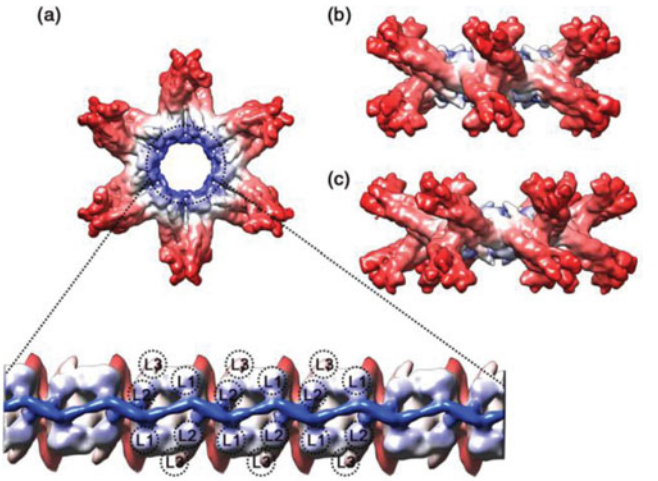


**Figure 4.** The cryo-EM electron density map of the central linker complex. (a) Top view along the molecular 6-fold axis. The density map is colored by radius with a red-to-blue spectrum. The electron densities found inside the black dashed circle unambiguously indicate the existence of the central bracelet structure which appears as a continuous sinusoid in the enlarged unwrapped planar map. (b) The complex viewed along a Q-dyad axis. (c) The complex viewed along a P-dyad axis.

from the $O_2$-bound and CO-bound states. By superimposing their structures, the local conformational changes within the subunit can be examined. One apparent structural change upon oxygenation is in the short coiled coil of L1 linker chain (see Figure 6(b)). The short coiled coil of L1 tilts toward the central plane with the hinge point near the inter-helical loop.

### *Interactions Between Protomers*

Except for the primary contacts made by the coiled coil domains, two distinct inter-ring and intra-ring contacts are formed between neighboring protomers. The most extensive inter-ring contacts occur along the Q-dyad. As shown in Figure 5(a), the $\beta$ barrel domains of L1 linker chain from two protomers pack together at the Q-dyad. The intra-ring contacts include interactions between globin dodecamers and the $\beta$ barrel domains of L2 and L3 linker chains (Figure 5(b)). The two hexagonal layers of *L. terrestris* Hb are partially staggered such that the architecture is more compact than the type II Hb [25]. Despite the closer manner of two hexagonal layers, the globin subunits actually do not have direct inter-ring interactions. It's the $\beta$ barrel domain of L1 linker chain providing the only inter-ring contacts, which could have an important role coordinating inter-ring allostery. Figure 6 shows the Q-dyad contact of L1 linker chains from different ligand-bound states. On going from CO to $O_2$-bound Hb, the $\beta$ barrel domains and the LDLR-like domain of both rings are translated outward from the center of the molecule. The translation of the Q-dyad contact is associated with the tilting of the short helix of the L1 coiled coil domain. The inter-helical loop of L1 linker chain seems to act as a flexible hinge to allow relative motion while maintaining the rigidity of the central linker complex.

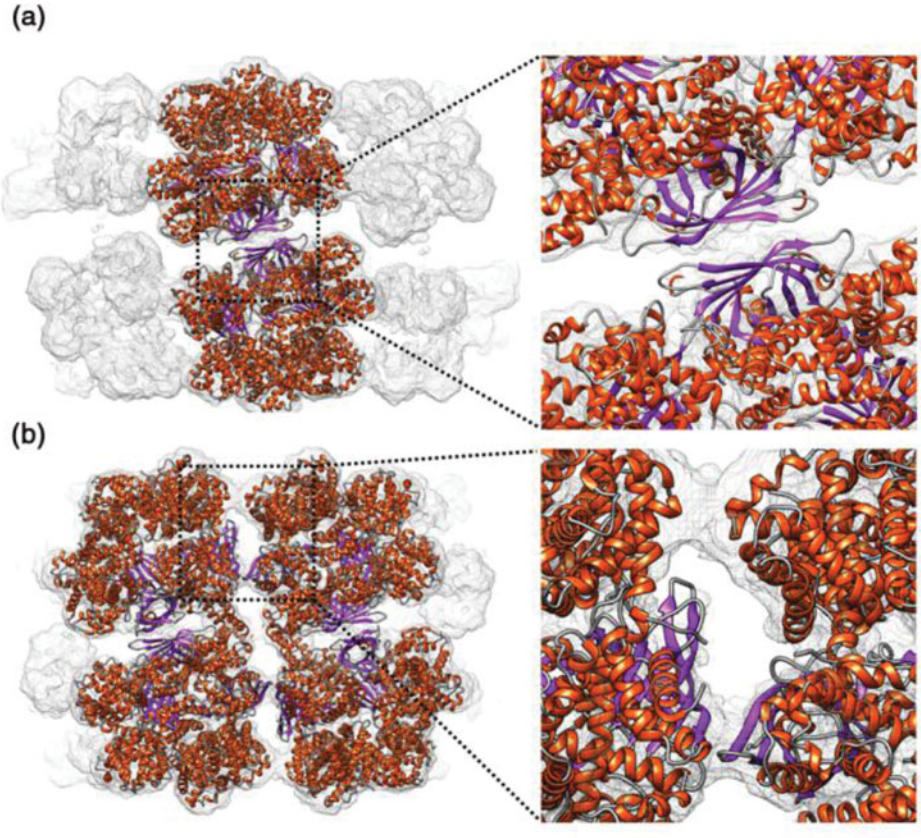


**Figure 5.** Contacts between protomers. (a) Inter-ring contacts along the Q-dyad. The model is colored by secondary structure with helix in orange red and strand in purple. (b) Intra-ring contacts between lateral protomers.

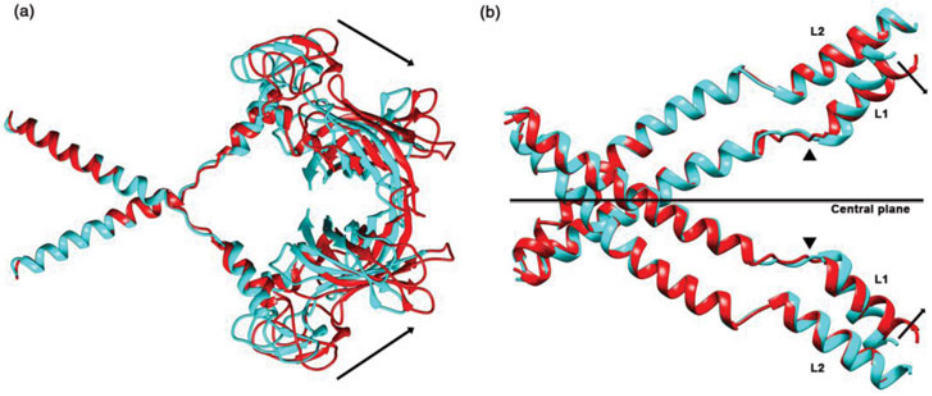


**Figure 6.** Comparison of the Q-dyad contact and coiled coil domain in CO-bound state (cyan) and $O_2$-bound state (red). (a) Comparison of the Q-dyad contact of L1 linker chains. The arrow indicates the transition direction of the $\beta$ barrel domains and the LDLR-like domains going from CO to $O_2$-bound state. (b) Comparison of the coiled coil domain. The tilt of the short coiled coil of L1 around the hinge point (marked by a triangle) near the inter-helical loop is indicated by an arrow.

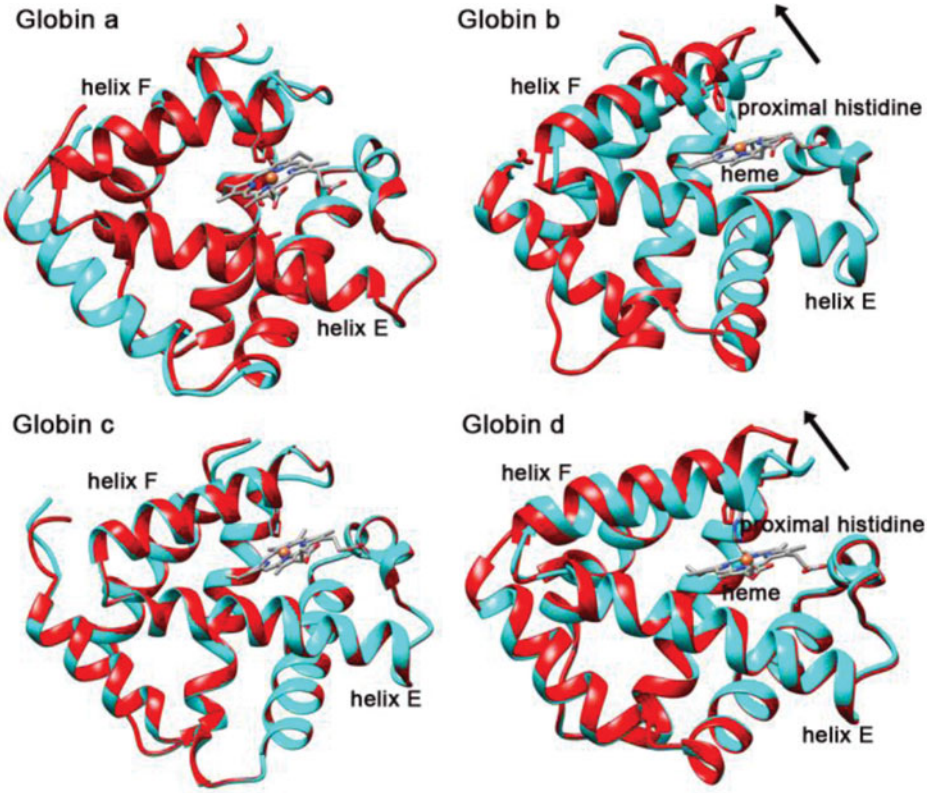


**Figure 7.** Comparison of the heme pocket of each globin subunit in CO-bound state (cyan) and $O_2$-bound state (red). The arrow indicates the tilting direction of helix F of globin b and globin d. The proximal histidine is away from the heme group in $O_2$-bound state.

### *Conformational Change in the Heme Pocket*

The extracellular *L. terrestris* Hb comprises four unique heme-containing subunits, a, b, c, and d in equal proportions. The four globin subunits exhibit the standard myoglobin fold, with seven $\alpha$ helices designated A through H (no D-helix) [7]. The heme group was contained in the E and F helices. Assembly of the globin dodecamer was dictated by four unique interfacial contacts, including two distinct EF dimer interfaces, one intra-tetramer interface and one inter-tetramer interface [7]. EF dimer pairing has been observed in all cooperative invertebrate hemoglobins to date [27], in which an extensive dimeric interface forms from contacts involving the heme containing E and F helices. In order to find the tertiary changes occurred in the heme pocket, we compared each globin subunit from the $O_2$-bound and CO-bound states. Their structures were superimposed for comparison and analyses (Figure 7). In this way, we can examine the local tertiary changes within the subunit, which is independent of the quaternary movement. In our results, one remarkable tertiary conformational change upon oxygen binding is in the helix F which contains the proximal histidine for interaction with the heme group. By interacting with the heme iron atom, the helix F tilts upward from the heme plane upon oxygen binding. Since we can not determine the location of the heme group by the cryo-EM map at this resolution, the heme

group is positioned relative to the CO-bound crystal structure. Interestingly, the tilt of the helix F only occurs in the subunit b and subunit d.

## 4. Discussion

The focus of our research was to investigate the structural transitions induced by different ligand binding to the giant hexagonal-bilayer Hb of *L. terrestris*. The combination of cryo-EM structure and the flexible fitting technique provides a good means for studying the tertiary and quaternary structure in the specific functional state. Earlier resonance Raman spectra [10] and small angle x-ray scattering studies [11] have previously pointed that the giant *L. terrestris* Hb lacked ligand-binding induced tertiary and quaternary changes. On the contrary, our results unambiguously indicate that the cooperative ligand binding of *L. terrestris* Hb requires both tertiary and quaternary allostery. Since the resonance Raman observations reflect an average behavior of all the heme pockets, it can not be ruled out that a small number of heme environments could undergo ligand-induced conformational change. Indeed, our results show that only the heme pocket in globin b and globin d undergoes tertiary changes. The distinctive feature in these two subunits could be due to the tryptophan at position B10 that reaches into the binding heme pocket, making van der Waals contacts with the gas ligand [7]. It is reasonable to attribute the tertiary changes to the interaction between the tryptophan and the gas ligand. The allosteric signal is transmitted through the heme iron to the proximal histidine, causing the tilting of helix F in globin b and d away from the heme plane. The structural transitions found here can fully explain the unusually high cooperativity of oxygen binding in the *L. terrestris* Hb. Here our results clearly show that the overall cooperativity of an hexagonal bilayer complex is caused by the plurality of subunit-subunit interactions in this assemblage, which is quite different from those of the vertebrate and other invertebrate Hbs. Besides the tertiary and quaternary allostery in the heme pocket, there is an alteration of the overall size of the complex. The oxygenation causes a radial expansion of the hexagonal-bilayer complex while maintaining the rigidity of the central linker complex. This global subunit movement is found to be accomplished by the allosteric communications between intra-ring and inter-ring contacts. The intra-ring interactions primarily involve main chain hydrogen bonding between $\beta$ barrel domains of L2 and L3 [6], while the inter-ring contacts involve the extensive packing of the $\beta$ barrel domains of L1 as seen in Figure 5(a). This emphasizes the critical role of linker chains in the allosteric behavior exhibited by this macromolecule. One interesting feature is the longest inter-helical segment of L1, which serves as a flexible hinge region (Figure 6(b)) that allows structural transitions of the short coiled coil relative to the longer one. The allosteric role of linker chains observed in our results provides a reasonable explanation for the smaller cooperativity of dodecamer [11] and Riftia Hb [28] without linker chains.

Another unanswered issue in the annelid Hb literatures concerns the presence of the additional densities in the central linker complex. The so-called "bracelet model" [13] had been proposed to explain the assembly of the quaternary structure by the central bracelet. Some of the early publications on *L. terrestris* Hb [5,12,15,29] provided some evidence of visible density in the center of the Hb macromolecule. The 5.5 Å resolution crystal structure [8] also revealed the plausible interdigitation of 12 triple-stranded coiled-coils near the center of the complex. The smaller central cavity and the sinusoidal pillars observed in the 14.9 Å cryo-EM structure [3] gave a further support of the additional densities which were absent in the crystal structure for unknown reasons. These findings, however, do not close the discussions because no detailed and complete structural evidence was provided so far. Our 8 Å resolution cryo-EM structure clearly reveals the details of the additional

sinusoidal bracelet that further enhance the completeness of the structural interdigitations between 12 triple-stranded coiled-coils. The absolute requirement for the L1 linker chain for the Hb assemblage and the interchangeability between L1 and L2 [29] also support the interdigitations between the extra densities (Figure 4(a)) and the L1 and L2 linker chains.

## 5. Conclusions

This study yields important implications for the cooperative mechanisms of the giant hexagonal bilayer Hb. The tertiary and quaternary allostery and the allosteric communications facilitated by intra-ring and inter-ring contacts underlie the requirement for distinct hemoglobin subunits and the non-heme linker chains. The flexibility of the $\beta$ barrel domain and the rigidity of the central linker complex strengthened by the extra bracelet clarify the dual functions of the linker chains. It remains to be seen what constituents could account for the additional sinusoidal densities. One possibility may be that the additional densities could correspond to the N-terminal residues of L1 and L2 linkers which were not observed in the crystal structure. Structural analysis at higher resolution will be required to elucidate how the allosteric signals transmit between the EF-dimer interfaces, how the allosteric units drive global movement, and how the structural transitions alter the oxygen binding affinity. The determination of the corresponding structures at specific functional states is a matter of vital importance.

## Acknowledgments

We warmly thank Profs. S. C. Lee, J. W. Chern, and C. R. Chang for supporting the Cryo-EM project in National Taiwan University.

## Funding

C.Y.C. acknowledges National Taiwan University and National Science Council (NSC-99-2112-M-002-013-MY3) for financial supports in this work.

## References

[1] Ackers G. K., & Holt J. M. (2006). *J Biol Chem*, *281*, 11441.
[2] Reichert E. T., & Brown A. P., (1908). *Exp Biol Med 5*, 66.
[3] Mouche F., Boisset N., & Penczek P. A. (2001). *J Struct Biol*, *133*, 176.
[4] Jouan L., Taveau J.-C., Marco S., Lallier F. H., & Lamy J. N. (2001). *J Mol Biol*, *305*, 757.
[5] Schatz M., Orlova E. V., Dube P., Jäger J., & van Heel M. (1995). *J Struct Biol*, *114*, 28.
[6] Royer W. E., Jr., Sharma H., Strand K., Knapp J. E., & Bhyravbhatla B. (2006). *Structure*, *14*, 1167.
[7] Strand K., Knapp J. E., Bhyravbhatla B., & Royer W. E., Jr. (2004). *J Mol Biol*, *344*, 119.
[8] Royer W. E., Jr., Strand K., van Heel M., & Hendrickson W. A. (2000). *Proc Natl Acad Sci USA*, *97*, 7107.
[9] Fushitani K., Imai K., & Riggs A. F. (1986). *J Biol Chem*, *261*, 8414.
[10] Vidugiris G. J., Harrington J. P., Friedman J. M., & Hirsch R. E. (1993). *J Biol Chem*, *268*, 26190.
[11] Krebs A., Kuchumov A. R., Sharma P. K., Braswell E. H., Zipper P., Weber R. E., Chottard G., & Vinogradov S. N. (1996). *J Biol Chem*, *271*, 18695.
[12] Ohtsuki M. & Crewe A. V. (1983). *J Ultrastruct Res*, *83*, 312.
[13] Vinogradov S. N., Lugo S. D., Mainwaring M. G., Kapp O. H., & Crewe A. V. (1986). *Proc Natl Acad Sci USA*, *83*, 8034.

[14] Lamy J. N., Green B. N., Toulmond A., Wall J. S., Weber R. E., & Vinogradov S. N. (1996). *Chem Rev*, *96*, 3113.
[15] de Haas F., Kuchumov A., Taveau J. C., Boisset N., Vinogradov S. N., & Lamy J. N. (1997). *Biochemistry*, *36*, 7330.
[16] Vinogradov S. N. & Sharma P. K. (1994). *Method Enzymol*, *231*, 112.
[17] Suloway C., Pulokas J., Fellmann D., Cheng A., Guerra F., Quispe J., Stagg S., Potter C. S., & Carragher B. (2005). *J. Struct. Biol.*, *151*, 41.
[18] Mindell J. A. & Grigorieff N. (2003). *J. Struct. Biol.*, *142*, 334.
[19] van Heel M., Harauz G., Orlova E. V., Schmidt R., & Schatz M. (1996). *J. Struct. Biol.*, *116*, 17.
[20] Tang G., Peng L., Baldwin P. R., Mann D. S., Jiang W., Rees I., & Ludtke S. J. (2007). *J. Struct. Biol.*, *157*, 38.
[21] Goddard T. D., Huang C. C., & Ferrin T. E. (2007). *J. Struct. Biol.*, *157*, 281.
[22] Topf M., Lasker K., Webb B., Wolfson H., Chiu W., & Sali A. (2008). *Structure*, *16*, 295.
[23] Pandurangan A. P. & Topf M. (2012). *J. Struct. Biol.*, *177*, 520.
[24] Suzuki T. & Riggs A. F. (1993). *J Biol Chem*, *268*, 13548.
[25] Royer W. E., Jr., Omartian M. N., & Knapp J. E. (2007). *J Mol Biol*, *365*, 226.
[26] Sali A., & Blundell T. L. (1993). *J. Mol. Biol.*, *234*, 779.
[27] Royer W. E., Jr., Zhu H., Gorr T. A., Flores J. F., & Knapp J. E. (2005). *J Biol Chem*, *280*, 27477.
[28] Arp A. J., Doyle M. L., Di Cera E., & Gill S. J. (1990). *Resp Physiol*, *80*, 323.
[29] Lamy J., Kuchumov A., Taveau J.-C., Vinogradov S. N., & Lamy J. N. (2000). *J Mol Biol*, *298*, 633.